Ab initio electronic relaxation times and transport in noble metals

Jamal I. Mustafa,[1,2] Marco Bernardi,[1,2,3] Jeffrey B. Neaton,[1,2,4,5] and Steven G. Louie[1,2,*]

[1]*Department of Physics, University of California, Berkeley, Berkeley, California 94720-7300, USA*
[2]*Materials Sciences Division, Lawrence Berkeley National Laboratory, Berkeley, California 94720, USA*
[3]*Department of Applied Physics and Materials Science, California Institute of Technology, Pasadena, California 91125, USA*
[4]*Molecular Foundry, Lawrence Berkeley National Laboratory, Berkeley, California 94720, USA*
[5]*Kavli Energy NanoSciences Institute at Berkeley, Berkeley, California 94720, USA*

Relaxation times employed to study electron transport in metals are typically taken to be constants and obtained empirically. Here, we use fully *ab initio* calculations to compute the electron-phonon relaxation times of Cu, Ag, and Au and find that they vary significantly on the Fermi surface, with values from ∼15 to 45 fs that are correlated with the Fermi surface topology. We compute room-temperature resistivities in excellent agreement with experiment by combining *GW* quasiparticle band structures, Wannier-interpolated band velocities, and *ab initio* relaxation times. We introduce an importance sampling scheme to speed up the convergence of resistivity and transport calculations.

Copper, silver, and gold are noble metals with broad application in electronics, power generation, catalysis, and plasmonics. They have attracted interest since the early days of solid state theory, as their electronic structure deviates from the free-electron model that applies to the alkali metals. The Fermi surface (FS) of noble metals is not spherical as in free-electron theory but is deformed due to the proximity of the *d* bands to the free-electron-like *sp* band [1–4]. Electron scattering processes at the FS are of particular relevance for noble metal applications, as they regulate charge and heat transport [5,6]. At room temperature in relatively pure metals, scattering with phonons [7,8] is dominant, while scattering with defects and impurities is important at low temperatures and in alloys or samples of low purity.

Transport in metals can be understood heuristically with the Drude theory [9], which assumes free electrons with a constant (that is, band- and **k**-independent) relaxation time (RT). Even in noble metals, where important deviations are expected from the Drude theory, resistive losses and optical experiments are routinely interpreted using constant relaxation times [9–11]. More advanced models, such as state-of-the-art *ab initio* calculations of resistivity and other transport properties [12,13], typically employ density functional theory (DFT) band structures combined with constant RTs inferred from experiment or estimated heuristically.

However, the RT of an electron in a Bloch state depends, in general, on the band and crystal momentum **k**, a point that has so far been often neglected. Accurate calculations of electron RTs are computationally costly, as they require fine Brillouin zone (BZ) sampling [14–16], prompting adoption of simplified schemes that employ either a constant RT [17] or an average scattering strength [18]. An exception are recent transport calculations in Al [19] and two-dimensional materials [19–21] that included the band and **k** dependence of the RTs.

As striking new experimental findings on noble metals emerge [22–24], predictive theories are needed to study electron scattering in these materials. For example, recent experiments by Kim *et al.* [22] show a remarkable resistivity drop when a single crystal of Ag is doped with a small fraction of Cu, contrary to the intuition that the resistivity should increase upon alloying due to enhanced impurity scattering. While the constant-RT approach may be too simplistic, at present it is not known whether more refined theories are necessary to improve our quantitative understanding of transport in the noble metals.

Here we compute electron-phonon (*e*-ph) RTs and *GW* band velocities of Cu, Ag, and Au on fine **k**-point grids. We develop a linear interpolation approach to sample **k** points directly on the FS and use it to study the correlation of the RTs and velocities with FS topology. We find that the *e*-ph RTs are far from constant on the FS. They vary by a factor of 2–3 between their minima and their maxima, located in FS regions with different curvatures. The band velocity maps on the FS exhibit anticorrelation with the *e*-ph RT maps. We investigate approximations to compute the resistivity of Cu, Ag, and Au at room temperature and find excellent agreement (within ∼10%) with experiment only when *ab initio* RTs and *GW* velocities are used. Our FS sampling approach dramatically speeds up the convergence of resistivity calculations and may be extended to study heat transport and thermoelectric effects in materials.

We carry out DFT calculations at experimental lattice constants (Cu: 3.61 Å, Ag: 4.09 Å, Au: 4.08 Å) using the local density approximation [25] and a plane-wave basis with the QUANTUM ESPRESSO code [26]. To determine the ground-state charge density, we use scalar-relativistic norm-conserving pseudopotentials [27] (including semicore *s* and *p* states), kinetic energy cutoffs of 240 Ry for Cu and 180 Ry for Ag and Au, and shifted 10^3-**k**-point grids. Spin-orbit effects are neglected. The quasiparticle energies are computed within the $G_0 W_0$ and generalized plasmon pole approximations [28,29] using the BERKELEYGW package [30]. Our *GW* calculations are well converged using a 50-Ry cutoff for the dielectric matrix, which was evaluated on an 8^3-**k**-point grid for interband transitions (finite **q**) and a 16^3-**k**-point grid for intraband transitions (**q** → 0) and using ∼1000 unoccupied bands, consistent with previous studies [31–33].

*sglouie@berkeley.edu

The e-ph matrix elements are computed on fine **k**-point grids with a procedure detailed in Ref. [16]. Briefly, we use density functional perturbation theory [34] to determine the phonon dispersions and displacement patterns, and the e-ph coupling matrix elements on a coarse $4 \times 4 \times 4$ **q**-point grid. The band structures, phonon dispersions, and e-ph matrix elements are interpolated using maximally localized Wannier functions [35–37] constructed from Bloch states on a 12^3-**k**-point grid. All quantities are interpolated using the EPW code [38,39] with our recently developed approach [14–16]. The velocities are calculated in the Wannier representation [40] using GW eigenvalues. For e-ph RT and resistivity calculations, we use the tetrahedron method [41] to obtain the FS as a collection of triangular facets, whose centroids constitute an ultrafine **k**-point grid employed in the calculations to sample the FS.

Following Mahan [8], the e-ph transport relaxation scattering rates $\Gamma_{n\mathbf{k}}$ (and their inverse, the RTs $\tau_{n\mathbf{k}} = \Gamma_{n\mathbf{k}}^{-1}$) are computed with perturbation theory, due to the interaction with phonons:

$$\Gamma_{n\mathbf{k}} = \frac{2\pi}{\hbar} \sum_{m\mathbf{q}\nu} |g_{nm,\nu}(\mathbf{k},\mathbf{q})|^2 (1 - \cos\theta_{\mathbf{k},\mathbf{k}+\mathbf{q}})$$
$$\cdot [(N_{\nu\mathbf{q}} + f_{m\mathbf{k}+\mathbf{q}}) \delta(\epsilon_{n\mathbf{k}} + \hbar\omega_{\nu\mathbf{q}} - \epsilon_{m\mathbf{k}+\mathbf{q}})$$
$$+ (N_{\nu\mathbf{q}} + 1 - f_{m\mathbf{k}+\mathbf{q}}) \delta(\epsilon_{n\mathbf{k}} - \hbar\omega_{\nu\mathbf{q}} - \epsilon_{m\mathbf{k}+\mathbf{q}})], \quad (1)$$

where $g_{nm,\nu}(\mathbf{k},\mathbf{q})$ are e-ph coupling matrix elements for an electron in Bloch state $|n\mathbf{k}\rangle$ (with quasiparticle energy $\epsilon_{n\mathbf{k}}$) that scatters into a Bloch state $|m\mathbf{k}+\mathbf{q}\rangle$ (with quasiparticle energy $\epsilon_{m\mathbf{k}+\mathbf{q}}$) due to a phonon with polarization ν, wave vector $\mathbf{q}$, and frequency $\omega_{\nu\mathbf{q}}$. Here, $\theta_{\mathbf{k},\mathbf{k}+\mathbf{q}}$ is the scattering angle between $\mathbf{k}$ and $\mathbf{k}+\mathbf{q}$. The two terms in brackets correspond to phonon absorption and emission, respectively, and the temperature dependence stems from the occupation factors $f_{n\mathbf{k}}$ and $N_{\nu\mathbf{q}}$, for electrons and phonons, respectively (in this work, both the electrons and the phonons are at 300 K). The conductivity tensor from Boltzmann transport theory within the relaxation-time approximation is expressed as the FS integral [5,8]

$$\sigma_{\alpha\beta} = \frac{2}{(2\pi)^3} \frac{e^2}{\hbar} \sum_n \int dS_F \frac{v_{n\mathbf{k},\alpha} v_{n\mathbf{k},\beta}}{|\mathbf{v}_{n\mathbf{k}}|} \tau_{n\mathbf{k}}, \quad (2)$$

where $v_{n\mathbf{k},\alpha}$ are Cartesian components ($\alpha = x,y,z$) of the velocities and $\tau_{n\mathbf{k}}$ e-ph RTs. The area elements dS_F correspond to the area of the triangular facets that make up the FS within our interpolation scheme. The resistivity ρ is obtained from the trace of the inverse of the conductivity tensor, i.e., $\rho = \text{Tr}[\sigma^{-1}]/3$ [42].

The computed Fermi surfaces (see Fig. 1) exhibit well-known [1–4] topological features, including open-orbit regions with upward curvature (known as "necks") near the L points of the BZ, spherical regions known as the "belly," as well as flatter regions near the K points between the necks, and "bulges" where the FS approaches the BZ edge at the X points. The FS of Ag is noticeably different from those of Cu and Au, with much smaller necks, less pronounced bulges, and an overall more spherical shape due to the d bands being lower in energy compared to Cu and Au.

Figure 1 shows maps of the e-ph RTs and GW velocities calculated at **k** points on the FS. For all three materials, we
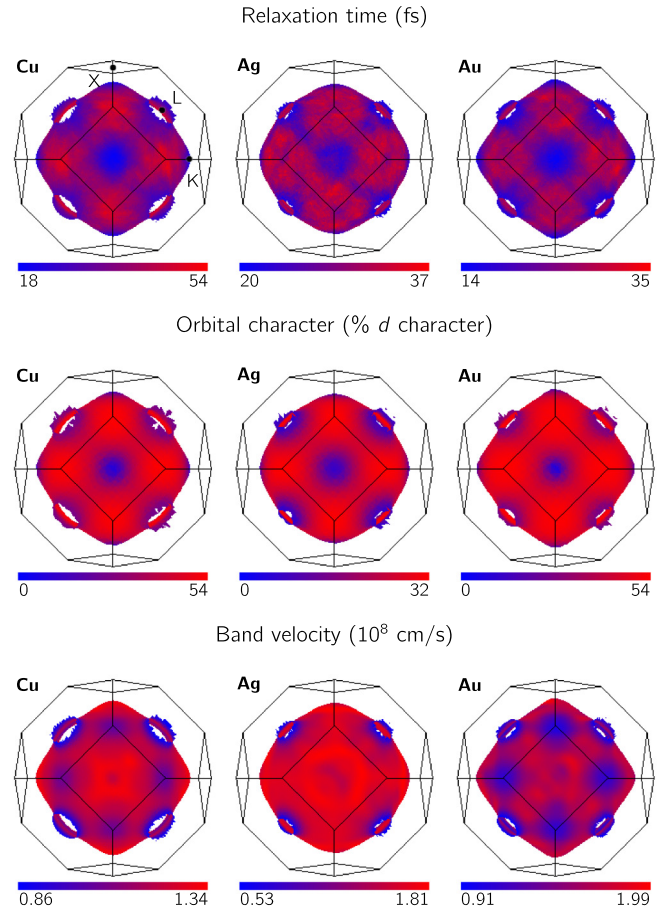

FIG. 1. Electron-phonon relaxation times (top), orbital character (middle), and band velocities (bottom) of states on the Fermi surface of Cu, Ag, and Au.

find large variations in the RTs, with the necks and bulges exhibiting shorter RTs than the belly and flat regions between the necks. The RTs vary the most in Cu and Au, with a factor of ~3 difference between the minima (located near the L and X points) and the maxima (located near the K point), while the variation in Ag is smaller, with only a factor of ~2 difference between minima and maxima. The velocities show an opposite trend, so that FS regions with longer (shorter) RTs are associated with lower (higher) velocities. Cu and Au exhibit moderate variations in the velocities, while Ag shows a large difference. The difference between the minimal velocities at the necks and the maximal velocities at the belly is a factor of ~2 in Cu and Au and a factor of ~4 in Ag.

We investigate the physical origin of the variation of the RTs and velocities on the FS. By mapping the orbital character of the electronic states on the FS (see Fig. 1), we find a correlation between the character of the state and its RT. Electronic states with a predominantly sp character, as found in the necks and bulges of the FS, are associated with shorter RTs, while states with large d character exhibit longer RTs.

In Fig. 2, we explore quantitatively the origin of the anisotropic RTs for the case of Ag, by choosing initial states with sp and $sp + d$ character, respectively, and computing the coupling matrix elements $|g|^2$ connecting these initial **k** points
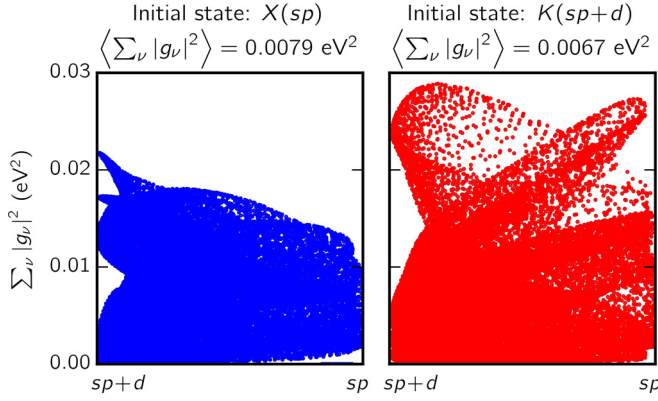
FIG. 2. Electron-phonon coupling matrix elements for an initial electronic state of predominantly sp character (left) and an initial state with large d character (right). Shown are the e-ph coupling matrix elements (summed over phonon polarizations) versus the character of the final electronic state involved in the e-ph scattering process. For each initial state, the average coupling matrix element is also given.

to all other final $\mathbf{k}$ points on the FS. These matrix elements are the ones entering the calculation of the RTs for each of the initial states within our approach [Eq. (1)], and we now seek to categorize them based on the character of the initial and final states in the e-ph scattering processes.

For an initial state near X with dominant sp character, the coupling, as measured by the sum over phonon polarizations of the matrix element between the initial and the final states, $\sum_\nu |g_\nu|^2$, is strongest to final states with d admixture along the [110] directions. We find that coupling to other final states with some d character is in general weaker and strongly anisotropic, so that different groups of final d-like states exhibit $|g|^2$ values distributed in multiple sets (see Fig. 2). As the fraction of d character of the final state decreases, the coupling decreases monotonically.

For an initial state near the K point with large d character, coupling is strong to one set of d-like states (along [110]) and weak to most other d-like states. Two distinct sets of $|g|^2$ values are found for such d-d coupling (see Fig. 2). As the d character of the final state decreases, different final states exhibit different trends: for some states the coupling becomes stronger, while for others it becomes weaker. On average, the $|g|^2$ is greater by a factor of 1.2 for the initial sp state near X, thus explaining the higher scattering rate (which is proportional to $|g|^2$) and shorter RT compared to states with large d character, as discussed above. While further investigation is needed to more completely understand the role of the character of the initial and final state and the perturbation potential, our results demonstrate that the e-ph matrix elements are highly anisotropic and depend strongly both on the character of the initial and final states and on the wave vector connecting the initial and final states through the perturbation potential induced by the phonons. The combination of these effects results in the anisotropic RTs found here. The variation in the velocities is easier to explain. It can be understood by considering the curvature of the FS: flatter regions have lower velocities compared to more curved regions, given that the latter are associated with a higher gradient of the band at the Fermi energy.

TABLE I. Comparison of relaxation times and velocities computed by averaging on the Fermi surface (headings in angle brackets) versus the same quantities obtained within Drude theory (headings with subscript D). The Fermi-surface-averaged relaxation times are computed using GW band structures, while the band velocities are given for both the DFT and the GW band structures for comparison. Drude values were obtained using Eq. (3) with resistivity experimental data [22,43] from single-crystal samples.

	τ (fs)		v (10^8 cm/s)		
	$\langle \tau_{n\mathbf{k}} \rangle$	τ_D	$\langle v_{n\mathbf{k}}^{\text{DFT}} \rangle$	$\langle v_{n\mathbf{k}}^{GW} \rangle$	v_D
Cu	37	27[a]	1.13	1.19	1.57
Ag	30	41[b]	1.45	1.55	1.39
Au	24	30[c]	1.38	1.52	1.39

[a]From Ref. [43].
[b]From Ref. [22].
[c]Using the estimated SC resistivity.

To highlight the difference between the *ab initio* and the empirical data, we compare in Table I the Fermi-surface-averaged RTs $\langle \tau_{n\mathbf{k}} \rangle$ and velocities $\langle v_{n\mathbf{k}} \rangle$, obtained by averaging the *ab initio* data in Fig. 1, with the values derived from the free-electron Drude model,

$$\tau_D = \frac{m^*}{ne^2\rho}, \quad v_D = \frac{\hbar(3\pi^2 n)^{1/3}}{m^*}, \tag{3}$$

where τ_D and v_D are the empirical Drude RT and free electron velocity, respectively. The *ab initio* average quantities $\langle X \rangle$ (with $X = \tau$, v) are computed over the triangular facets that compose the FS, using $\sim 10\,000$ $\mathbf{k}$ points and weighing by the facet area,

$$\langle X \rangle = \frac{\sum_t A_t X_{\mathbf{k}_c}}{\sum_t A_t}, \tag{4}$$

with A_t the facet area for a triangle t and $\mathbf{k}_c$ its centroid. The Drude RTs τ_D are calculated using the resistivity ρ measured on single-crystal (SC) samples [22,43] (see Table II); we further obtain the charge density n using one free electron per unit cell and take the effective mass $m^* = m_e$, consistent with

TABLE II. Resistivity values (in units of $\mu\Omega$ cm) at 300 K computed using GW band velocities and different approximations for the relaxation times: $\tau_{n\mathbf{k}}$ are band and $\mathbf{k}$ dependent relaxation times from *ab initio* data, $\langle \tau_{n\mathbf{k}} \rangle$ are Fermi surface averages of the $\tau_{n\mathbf{k}}$'s, and τ_D are empirical Drude relaxation times. Also listed are the resistivity values computed from DFT velocities and empirical Drude relaxation times. Experimental data for single-crystal (SC) and polycrystalline (PC) samples are listed for comparison.

	Computed ρ				Experimental ρ	
	$\tau_{n\mathbf{k}}$	$\langle \tau_{n\mathbf{k}} \rangle$	τ_D	DFT + τ_D	SC	PC
Cu	1.51	1.51	2.05	2.19	1.52[a]	1.67[a]
Ag	1.81	1.83	1.34	1.43	1.49[b]	1.59[b]
Au	2.24	2.24	1.82	2.01	2.0[c]	2.26

[a]From Ref. [43].
[b]From Ref. [22].
[c]Estimated from the PC resistivity.

a simple Drude treatment of noble metals [9]. We find that the $\langle \tau_{n\mathbf{k}} \rangle$ of Cu is 50% larger than the Drude value, while the $\langle \tau_{n\mathbf{k}} \rangle$'s of Ag and Au are 15%–25% smaller than their respective Drude RTs. The magnitude of the velocities averaged over the FS show the opposite behavior, with $\langle v_{n\mathbf{k}} \rangle$ smaller in Cu and larger in Ag and Au than the Drude value. These results challenge the accuracy of the widely used empirical Drude model. In particular, since the tabulated Drude RTs are constants, they miss the complex trends and significant variation on the FS found here. The Drude RTs should thus be regarded as mere model parameters used to interpret transport and optical experiments in the absence of *ab initio* data.

Next, we use our results to compute the resistivity of Cu, Ag, and Au, with a range of approximations for the RTs and velocities. Table II compares the resistivities calculated with the *GW* velocities in combination with (i) full band- and **k**-resolved RTs $\tau_{n\mathbf{k}}$, (ii) FS-averaged *ab initio* RTs $\langle \tau_{n\mathbf{k}} \rangle$, and (iii) empirical Drude RTs τ_D. For comparison, we also compute the resistivities using the common approach combining DFT (as opposed to *GW*) velocities with Drude RTs. We compare our calculated resistivities with experiments at 293 K for SC samples. Polycrystalline (PC) experimental data [44] are also given. Since in pure SC samples at room temperature the source of resistivity is almost exclusively *e*-ph scattering, our approach using *e*-ph RTs is justified.

We first discuss the data in Table II obtained with our best approximation, namely, *ab initio* $\tau_{n\mathbf{k}}$ and *GW* velocities. In the case of Cu, the agreement with SC experiment is excellent (within 1%). For Ag and Au we find resistivities that are higher by ∼10% than experiment. We attribute this small discrepancy to a number of sources, including the ∼0.1-eV accuracy of the quasiparticle energies obtained via the *GW* method and a ∼5% uncertainty in the RTs depending on whether or not the cosine factor in Eq. (1) is employed [8]. Using the average RTs $\langle \tau_{n\mathbf{k}} \rangle$ with *GW* velocities gives nearly identical resistivities as the band- and **k**-resolved RTs, thus suggesting that approximate schemes using a constant RT should employ FS-averaged *ab initio* data rather than empirical data.

For all three materials, we find that the velocities obtained from the *GW* quasiparticle band structures are ∼10% higher than those obtained via DFT (see Table I), consistent with previous studies in Au [33] showing a large effect of *GW* on the *d*-band energies and *sp* band width. For Ag and Au, the lower DFT velocities, combined with Drude RTs that are larger than the *ab initio* values, yield resistivities in fortuitous agreement with experiment when using the DFT velocity plus τ_D approach, a result of compensation of errors. For Cu, on the other hand, the DFT velocity plus τ_D approach gives a resistivity almost 50% higher than experiment. Our results highlight the predictive character of calculations combining *GW* band structures and velocities with *ab initio* *e*-ph RTs.

The resistivity calculations in Table II are obtained with a novel approach that employs direct FS sampling instead of a homogeneous **k** grid in the BZ, affording orders of magnitude speed up the convergence of the resistivity with respect to the number of **k**-points. Figure 3 compares the convergence of the resistivity with respect to number of **k**-points for uniform and importance sampling. Since we focus only on the convergence behavior with respect to number of **k**-points, the resistivity, for illustration in Fig. 3, is determined using DFT velocities and
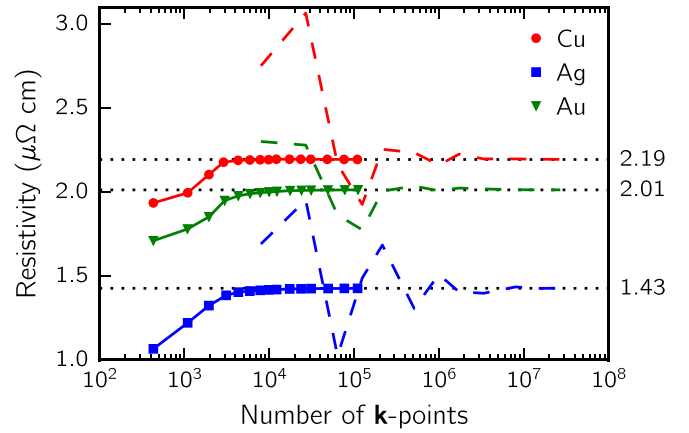

FIG. 3. Convergence of the resistivity computed with a uniform $\vec{k}$-grid (dashed lines) and using Fermi surface importance sampling (solid line with markers). The dotted lines indicate the converged values.

τ_D, though the trends are general. We find that the importance sampling scheme reaches convergence for ∼10^4 **k**-points and approaches monotonically the converged value. On the other hand, the commonly employed uniform grid requires ∼10^7 **k**-points to converge and fluctuates considerably with increasing number of **k**-points as it approaches convergence. Since calculations of *e*-ph relaxation times are computationally expensive, the importance sampling scheme provides great advantages when *ab initio* relaxation times are employed. For the noble metal cases discussed here, importance sampling decreases the number of **k**-points in the *e*-ph relaxation time calculation by a factor of 10^3. When higher order terms in the Sommerfeld expansion are needed, e.g. to compute high temperature electrical resistivity or thermal conductivity and thermopower, additional isoenergy surfaces (at $E_F \pm dE$) can be computed with a small computational overhead. Our approach is thus highly promising for computing transport properties beyond the resistivity.

In conclusion, we show that the *e*-ph RTs and velocities vary considerably on the FS of Cu, Ag, and Au. The correlation between RTs, velocities, and FS topology found here may extend to other classes of materials with complex Fermi surfaces. Our work points out the shortcomings of employing empirical RTs, DFT bands, and uniform **k** grids to compute transport properties in materials. It further suggests that even energy-dependent (but not **k**-dependent) RTs, also commonly employed in transport studies, would miss the complex interplay of band structure and scattering processes. These observations may extend to defect and impurity scattering, which will be the subject of future investigations. While complex nonequilibrium approaches are being explored for carrier dynamics, we argue that accurate *ab initio* state-dependent RTs may yield a close agreement with experiment in many cases of practical interest, even within the RT approximation of the Boltzmann transport equation.

[1] D. Shoenberg, Philos. Trans. R. Soc. London A **255**, 85 (1962).

[2] D. J. Roaf, Philos. Trans. R. Soc. London A **255**, 135 (1962).

[3] A. S. Joseph and A. C. Thorsen, Phys. Rev. Lett. **13**, 9 (1964).

[4] M. R. Halse, Philos. Trans. R. Soc. London A **265**, 507 (1969).

[5] J. M. Ziman, *Electrons and Phonons* (Oxford University Press, New York, 1960).

[6] T. P. Beaulac, P. B. Allen, and F. J. Pinski, Phys. Rev. B **26**, 1549 (1982).

[7] L. Sham and J. Ziman, in *The Electron-Phonon Interaction. Solid State Physics* (Academic Press, New York, 1963), Vol. 15, pp. 221–298.

[8] G. D. Mahan, *Condensed Matter in a Nutshell* (Princeton University Press, Princeton, NJ, 2010).

[9] N. W. Ashcroft and N. D. Mermin, in *Solid State Physics* (Saunders, Philadelphia, 1976), p. 293.

[10] J. B. Khurgin and A. Boltasseva, MRS Bull. **37**, 768 (2012).

[11] P. B. Johnson and R.-W. Christy, Phys. Rev. B **6**, 4370 (1972).

[12] G. Pizzi, D. Volja, B. Kozinsky, M. Fornari, and N. Marzari, Comput. Phys. Commun. **185**, 422 (2014).

[13] G. K. Madsen and D. J. Singh, Comput. Phys. Commun. **175**, 67 (2006).

[14] M. Bernardi, D. Vigil-Fowler, J. Lischner, J. B. Neaton, and S. G. Louie, Phys. Rev. Lett. **112**, 257402 (2014).

[15] M. Bernardi, D. Vigil-Fowler, C. S. Ong, J. B. Neaton, and S. G. Louie, Proc. Natl. Acad. Sci. USA **112**, 5291 (2015).

[16] M. Bernardi, J. Mustafa, J. B. Neaton, and S. G. Louie, Nat. Commun. **6** 7044 (2015).

[17] D. Parker and D. J. Singh, Phys. Rev. B **82**, 035204 (2010).

[18] S. Y. Savrasov and D. Y. Savrasov, Phys. Rev. B **54**, 16487 (1996); S. Y. Savrasov, D. Y. Savrasov, and O. K. Andersen, Phys. Rev. Lett. **72**, 372 (1994).

[19] W. Li, Phys. Rev. B **92**, 075405 (2015).

[20] C.-H. Park, N. Bonini, T. Sohier, G. Samsonidze, B. Kozinsky, M. Calandra, F. Mauri, and N. Marzari, Nano Lett. **14**, 1113 (2014).

[21] X. Li, J. T. Mullen, Z. Jin, K. M. Borysenko, M. Buongiorno Nardelli, and K. W. Kim, Phys. Rev. B **87**, 115418 (2013).

[22] J. Y. Kim, M.-W. Oh, S. Lee, Y. C. Cho, J.-H. Yoon, G. W. Lee, C.-R. Cho, C. H. Park, and S.-Y. Jeong, Sci. Rep. **4**, 5450 (2014).

[23] J. S. Fakonas, H. Lee, Y. A. Kelaita, and H. A. Atwater, Nat. Photon. **8**, 317 (2014).

[24] J. J. Paggel, D.-A. Luh, T. Miller, and T.-C. Chiang, Phys. Rev. Lett. **92**, 186803 (2004).

[25] J. P. Perdew and A. Zunger, Phys. Rev. B **23**, 5048 (1981).

[26] P. Giannozzi, S. Baroni, N. Bonini, M. Calandra, R. Car, C. Cavazzoni, D. Ceresoli, G. L. Chiarotti, M. Cococcioni, I. Dabo *et al.*, J. Phys.: Condens. Matter **21**, 395502 (2009).

[27] N. Troullier and J. L. Martins, Phys. Rev. B **43**, 1993 (1991).

[28] L. Hedin and S. Lundqvist, in *Effects of Electron-Electron and Electron-Phonon Interactions on the One-Electron States of Solids. Solid State Physics*, edited by D. T. Frederick Seitz and H. Ehrenreich (Academic Press, New York, 1970), Vol. 23, pp. 1–181.

[29] M. S. Hybertsen and S. G. Louie, Phys. Rev. B **34**, 5390 (1986); S. G. Louie, in *Conceptual Foundations of Materials: A Standard Model for Ground- and Excited-State Properties. Contemporary Concepts of Condensed Matter Science*, edited by S. G. Louie and M. L. Cohen (Elsevier, Amsterdam, 2006), Vol. 2, pp. 9–53.

[30] J. Deslippe, G. Samsonidze, D. A. Strubbe, M. Jain, M. L. Cohen, and S. G. Louie, Comput. Phys. Commun. **183**, 1269 (2012).

[31] A. Marini, G. Onida, and R. Del Sole, Phys. Rev. Lett. **88**, 016403 (2001).

[32] I. Tamblyn, P. Darancet, S. Y. Quek, S. A. Bonev, and J. B. Neaton, Phys. Rev. B **84**, 201402 (2011).

[33] T. Rangel, D. Kecik, P. E. Trevisanutto, G.-M. Rignanese, H. Van Swygenhoven, and V. Olevano, Phys. Rev. B **86**, 125125 (2012).

[34] S. Baroni, S. de Gironcoli, A. Dal Corso, and P. Giannozzi, Rev. Mod. Phys. **73**, 515 (2001).

[35] N. Marzari and D. Vanderbilt, Phys. Rev. B **56**, 12847 (1997).

[36] I. Souza, N. Marzari, and D. Vanderbilt, Phys. Rev. B **65**, 035109 (2001).

[37] A. A. Mostofi, J. R. Yates, Y.-S. Lee, I. Souza, D. Vanderbilt, and N. Marzari, Comput. Phys. Commun. **178**, 685 (2008).

[38] J. Noffsinger, F. Giustino, B. D. Malone, C.-H. Park, S. G. Louie, and M. L. Cohen, Comput. Phys. Commun. **181**, 2140 (2010).

[39] F. Giustino, M. L. Cohen, and S. G. Louie, Phys. Rev. B **76**, 165108 (2007).

[40] J. R. Yates, X. Wang, D. Vanderbilt, and I. Souza, Phys. Rev. B **75**, 195121 (2007).

[41] G. Lehmann and M. Taut, Phys. Status Solidi B **54**, 469 (1972); A. H. MacDonald, S. H. Vosko, and P. T. Coleridge, J. Phys. C **12**, 2991 (1979); P. E. Blöchl, O. Jepsen, and O. K. Andersen, Phys. Rev. B **49**, 16223 (1994).

[42] We note that Eq. (2) is valid at temperatures much lower than the Fermi temperature E_F/k_B, as is the case for noble metals at room temperature.

[43] Y. C. Cho, S. Lee, M. Ajmal, W.-K. Kim, C. R. Cho, S.-Y. Jeong, J. H. Park, S. E. Park, S. Park, H.-K. Pak, and H. C. Kim, Crystal Growth Design **10**, 2780 (2010).

[44] For Cu and Ag, resistivity measurements on SC samples [43,22] show an ∼10% reduction compared to PC samples (see Table II). We assume a similar reduction in the case of SC Au in order to obtain an estimate of the SC resistivity, which we could not find in the literature.